Optimal Position and Orientation Study of Reconfigurable Intelligent Surfaces in a Mobile User Environment

Giorgos Stratidakis, *Member, IEEE*, Sotiris Droulias, and Angeliki Alexiou, *Member, IEEE*

***Abstract*— Reconfigurable intelligent surfaces (RISs) have been often proposed as a means for restoring nonline-of-sight links in wireless communications. Because the path loss changes with the relative distance of the RIS from the transmitter and the receiver and their relative orientations, the quality of the communication is expected to depend strongly on the RIS placement in an RIS-aided link. In this work, the optimal placement of the RIS is studied with respect to both position and orientation and it is shown that even for an ideal RIS, i.e., lossless, polarization preserving, and with a uniform response with respect to the incident angle, the quality of the communication is greatly affected by the RIS orientation. To provide insight into the optimal choice, the analysis is based on an analytical model that treats the RIS as a continuous surface of finite size that steers the incident beam toward a prescribed direction. By imposing a desired minimum threshold on the received power, it is studied how the efficiency of the RIS depends on both its position and orientation. The decisions that have to be made concerning the placement of the RIS are illustrated with examples of D-band indoor scenarios.**

***Index Terms*— Beam steering, millimeter wave (mmWave), reconfigurable intelligent surfaces (RISs), RIS efficiency, RIS orientation, RIS placement, terahertz (THz).**

I. Introduction

IN RECENT years, reconfigurable intelligent surfaces (RISs) have been extensively studied as a means to mitigate the increased path loss [1] and blockage [2], [3], [4] that are met at high-frequency bands, such as the millimeter-wave (mmWave) and terahertz (THz) frequency bands. Their ability to steer beams toward selected directions with low power requirements, in contrast e.g., to relays [5], and without using active elements that amplify additive white Gaussian noise (AWGN) [6], is especially attractive. However, in view of the available choices for the RIS placement, the propagation path is not uniquely determined and, in order to achieve the desired communication quality, the position and orientation of the RIS, with respect to the location of the transmitter [or access point (AP)] and the receiver [or user equipment (UE)], must be thoroughly studied.

Manuscript received 4 February 2022; revised 4 August 2022; accepted 11 September 2022. Date of publication 26 September 2022; date of current version 9 November 2022. This work was supported by the European Commission's Horizon 2020 Research and Innovation Programme under Grant 871464 [Artificial Intelligence Aided D-band Network for 5G Long Term Evolution (ARIADNE)]. *(Corresponding author: Giorgos Stratidakis.)*

The authors are with the Department of Digital Systems, University of Piraeus, 18532 Piraeus, Greece (e-mail: giostrat@unipi.gr; sdroulias@unipi.gr).

Color versions of one or more figures in this article are available at https://doi.org/10.1109/TAP.2022.3208036.

Digital Object Identifier 10.1109/TAP.2022.3208036

So far, several studies have been devoted to the assessment of the optimal RIS placement with respect to the position of the AP and the UE [7], [8], [9], [10], [11], [12], [13], [14], [15]. Ntontin *et al.* [7] studied the optimal RIS placement in regard to the signal-to-noise ratio (SNR) at the receiver. They show that when the beam footprint of the AP on the RIS is much larger than the RIS, the optimal RIS placement can be close to the AP, close to the UE, or in the middle of the AP-UE line. When the footprint is at most equal to the RIS, the optimal RIS placement is close to the UE. Ibrahim *et al.* [8] studied the optimal position of the RIS in different propagation environments for single-input-single-output (SISO) and multiple-input–multiple-output (MIMO) communications. They show that for SISO communications, the RIS should be deployed near the transmitter or the receiver. For MIMO communications, in line-of-sight (LoS) environments, the RIS can be placed near or far from the transmitter and the receiver and yield considerable rate gain, while in non-LoS (nLoS) environments, the RIS should be placed near the transmitter or the receiver. Lu *et al.* [9] focused on jointly optimizing the transmit beamforming and the placement and phase shifts of the aerial RISs, in order to maximize the worst case SNR. In [10], a deployment strategy is revealed with the purpose of minimizing the blockage probabilities of the base station (BS)-user and RIS-user links. Hashida *et al.* [11] optimized the placement of the RISs, in order to support aerial users in terms of coverage and signal-to-interference-plus-noise ratio (SINR). In [12], two RIS deployment strategies are explored. In the first one, two RISs of $M/2$ elements each are deployed near two users, and in the second one, RIS of M elements is deployed near the AP. In [13], a general form of the SNR coverage probability is derived by considering the number and size of the RIS elements, along with the position of the RIS.

While the study of the optimal RIS position has been the subject of several works, the RIS orientation has been so far largely unexplored. In [14], the BS–RIS distance and the RIS orientation are optimized with respect to the cell coverage and the authors conclude that the optimal orientation is the RIS being deployed vertically to the BS-RIS line. However, the theoretical analysis in [14] fails to provide some insight on the particular choices with respect to the receiver. Only in the recent work [15], the optimal RIS placement is studied in conjunction with the orientation of the RIS, in order to maximize the minimum power at the receiver within a typical room in a D-band indoor scenario.

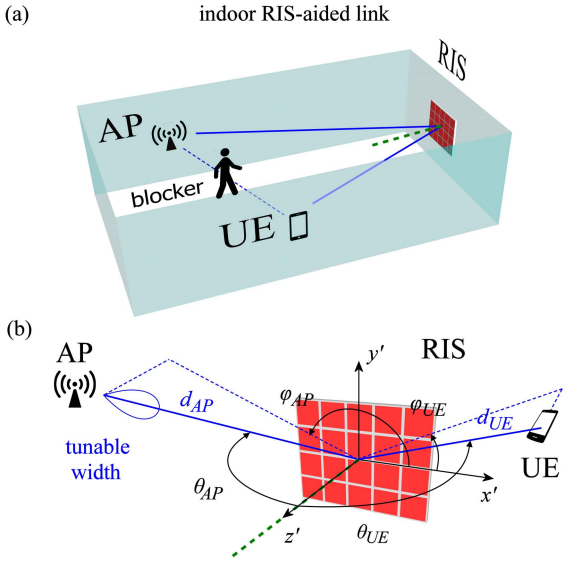

Fig. 1. System model of an indoor RIS-aided link. (a) Blocker interrupts the LoS communication link between the AP and the UE (blue dashed line) and the connection is restored via the RIS, which steers the AP beam toward the UE (blue solid lines). The green dashed line marks the normal to the RIS surface. (b) Schematic of the positions and relative angles between the AP, RIS, and UE, expressed on the local coordinate system of the RIS. The RIS elements are represented by the red rectangles.

In this work, the placement of the RIS is studied thoroughly with respect to both position and orientation. In order to provide insight into the optimal choices that have to be made, the analytical model developed in [16] is here employed. According to this model, a beam scattered from the RIS results from the global response of the RIS, which is modeled as a continuous surface, rather than from the collective response of local scatterers (RIS elements) as in [7], [8], [9], [10], [11], [12], [13], and [14]. Therefore, this treatment is ideal for gaining insight into how a beam is redirected by the RIS, thus facilitating the understanding of how the incident power is redistributed in the available space and, consequently, how the choices for the optimal RIS placement have to be made. By imposing a desired minimum threshold on the received power, it is found that the efficiency of the RIS depends on both its position and orientation, even for an ideally lossless RIS. The decisions that have to be made concerning the positioning of the RIS in an RIS-aided link are illustrated with examples of D-band indoor scenarios.

II. System Model

The system model of an RIS-aided link is shown in Fig. 1(a). The AP is equipped with a highly directional antenna with tunable beamwidth and illuminates the RIS, which subsequently steers the incident beam to any desired direction. As shown in Fig. 1(b), the AP is located at distance d_{AP} from the RIS center, with elevation angle θ_{AP} and azimuth angle ϕ_{AP} from the RIS to the AP, expressed on the RIS local coordinate system $x'y'z'$. The beam steering is achieved by tuning the RIS elements (red-colored rectangles in Fig. 1(b), periodically repeated along the x'- and y'-directions) to impose a prescribed phase shift on the incident beam. Here, the RIS steers the beam toward the UE, which is located at distance d_{UE} from the RIS center, with elevation angle θ_{UE} and azimuth angle ϕ_{UE} from the RIS to the UE. The flat surface of the RIS makes it ideal for placement on a wall, as shown schematically in the typical indoor scenario of Fig. 1.

To calculate the power received by the UE, P_r, one needs to know the power density, S_r, at the UE position and the effective aperture of the UE, A_r

$$P_r = S_r A_r. \tag{1}$$

The effective aperture of the UE is simply given by $A_r = G_r\lambda^2/4\pi$, where G_r is the antenna gain of the UE and λ is the free-space wavelength. For the calculation of S_r, typically, the contribution from each unit cell to the total electric field at the UE position is required, leading to an E-field summation over all unit cells, as adopted in several works [17], [18]. Alternatively, due to the subwavelength nature of the RIS elements (usually in the order of $\lambda/5$ or less), the RIS can be treated as a continuous surface [16]. The advantage of this approach over the E-field summation is that the E-field of the steered beam can be expressed in a simple closed form, thus offering a direct visualization of the spatial redistribution of the incident power and enabling the derivation of analytical expressions that provide insight into the operation of the RIS. This technique is particularly useful for pencil beams produced by highly directional antennas, where the entire AP beam is captured by the RIS, and the beam from the AP to the UE can be therefore described entirely by a continuous distribution.

In many cases where the goal is the RIS design, theoretical works focus on determining the RIS element properties (surface electric, magnetic, and possibly magnetoelectric conductivities) that transform the incident wave to a reflected wave with the desired, modified properties (e.g., direction, polarization, and amplitude) [19], [20], [21], [22]. Here, the starting point is an RIS that already has these necessary properties to perform steering; hence, this work focuses on the properties of the reflected beam and how these relate to the power redistribution of the incident beam in space that undergoes steering by the RIS. To this end, let the elevation and azimuth angles θ_r and ϕ_r from the RIS, respectively, define the direction along which the RIS steers the incident beam, and $(x_0, y_0, z_0) = (r_0 \sin\theta_0 \cos\phi_0, r_0 \sin\theta_0 \sin\phi_0, r_0 \cos\theta_0)$ be an observation point defined with respect to the local coordinate system of the RIS, where $r_0 = \sqrt{x_0^2 + y_0^2 + z_0^2}$. Using a Gaussian distribution to describe the main lobe of the AP antenna, in [16], it was shown that the power density at the observation point (x_0, y_0, z_0) that is due to the beam that is reflected by the RIS toward the direction defined by the angles θ_r and ϕ_r is given by

$$S_r = \frac{\frac{2P_t}{\lambda z_R}|R|^2}{\sqrt{\left(1+\frac{z_r^2}{z_R^2}\right)\left(1+\frac{z_r^2}{z_R^2\cos^4\theta_r}\right)}} \exp^{-\frac{k_0}{z_R}\Psi} \tag{2}$$

where

$$\Psi = \frac{x_r^2 + y_r^2}{\left(1 + \frac{z_r^2}{z_R^2}\right)} - \frac{(1 - \cos^4\theta_r)(x_r \cos\phi_r + y_r \sin\phi_r)^2}{\left(1 + \frac{z_r^2}{z_R^2}\right)\left(1 + \frac{z_R^2 \cos^4\theta_r}{z_r^2}\right)} \quad (3)$$

and

$$x_r = x_0 - z_r \sin\theta_r \cos\phi_r \quad (4a)$$

$$y_r = y_0 - z_r \sin\theta_r \sin\phi_r \quad (4b)$$

$$z_r = z_0 / \cos\theta_r. \quad (4c)$$

Note that P_t is the total power of the incident beam, $|R|$ is the common reflection amplitude of all RIS elements, and z_R is the Rayleigh length, which can be expressed in terms of $k = 2\pi/\lambda$, the free-space wavenumber, and either w_{RIS}, the AP beam footprint radius on the RIS, or G_t, the AP antenna gain, as [16]

$$z_R = \frac{k w_{RIS}^2}{2} = \frac{4k d_{AP}^2}{G_t}. \quad (5)$$

The model of (2)–(5) captures the basic and important features of the RIS, i.e., it performs beam steering. It is derived directly from Maxwell's equations (it is an asymptotically exact Gaussian beam solution to the 3-D scalar Helmholtz equation [23]) with the only assumptions that: 1) the RIS is a continuous surface that is larger than the beam footprint; 2) the RIS preserves the polarization of the incident beam, which is either transverse electric (TE) or transverse magnetic (TM); and 3) after reflection from the RIS, the incident beam remains a beam with the same qualitative properties, i.e., an incident Gaussian beam is reflected as a Gaussian beam of possibly different power (it does not split or diffuse). Note that this model predicts the power distribution everywhere in space, contrary to many works where the results are restricted to the far field only (the latter is typical to finite-sized RISs being fully illuminated, essentially forming a radiating aperture, with the far field being determined by the size of the aperture, i.e., the RIS size). In addition, because the incident wave is here modeled as a beam rather than a plane wave, as usually considered in most other relevant works, the impact of the AP beam on the RIS performance is also introduced [(5) captures the impact of the AP beam gain and AP-RIS distance on the Rayleigh length, which determines the transition from the near field to the far field of the reflected beam].

Using (1) and with the aid of (2)–(5), one can calculate the power received by the UE, i.e., at the observation point (x_{UE}, y_{UE}, z_{UE}), where $x_{UE} = d_{UE} \sin\theta_{UE} \cos\phi_{UE}$, $y_{UE} = d_{UE} \sin\theta_{UE} \sin\phi_{UE}$, and $z_{UE} = d_{UE} \cos\theta_{UE}$, in spherical coordinates. The UE is not necessarily located along the steering direction, i.e., $\theta_r \neq \theta_{UE}$ and $\phi_r \neq \phi_{UE}$, and in this case, the beam reflected by the RIS and the UE is misaligned. Apparently, the received power increases as the steering direction approaches the UE position and is maximized when $\theta_r = \theta_{UE}$ and $\phi_r = \phi_{UE}$. This is the case where misalignment between the RIS beam and AP antenna is eliminated and exactly at (x_{UE}, y_{UE}, z_{UE}), where $x_r = 0$, $y_r = 0$, and $z_r = d_{UE}$ [see (4)], and the power density is simply

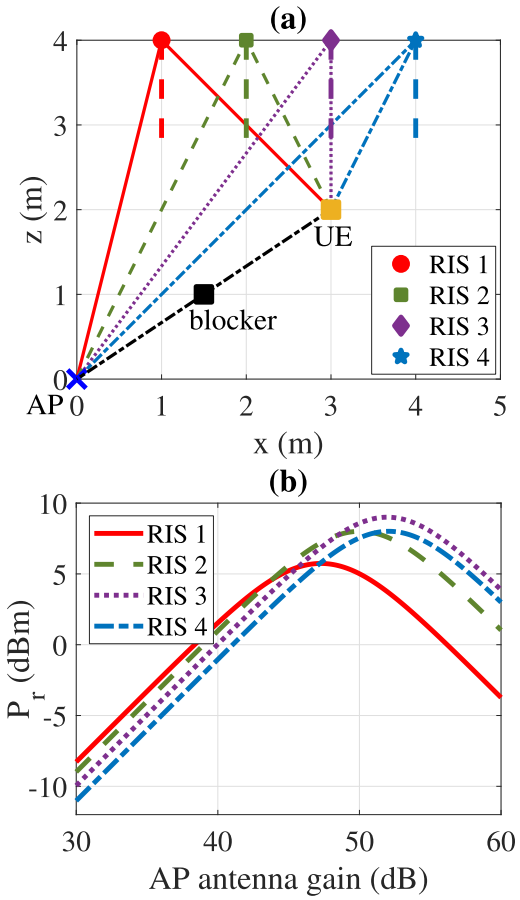

Fig. 2. Study of RIS placement in an indoor scenario for a static UE. (a) Scenario, presenting a 4 × 5 m room with fixed positions for the AP and UE. Only the top wall is available for the RIS placement. The black dashed-dotted line shows the LoS path, which is interrupted by a blocker. The vertical dashed lines depict the normal to the RIS surface and the rest of the colored lines denote the restored propagation path from the AP to the UE for variable RIS positions. (b) Power received by the UE as a function of the AP antenna gain (G_t), for the four selected RIS positions shown in (a).

given by

$$S_r = \frac{\frac{2P_t}{\lambda z_R}|R|^2}{\sqrt{\left(1 + \frac{d_{UE}^2}{z_R^2}\right)\left(1 + \frac{d_{UE}^2}{z_R^2 \cos^4\theta_{UE}}\right)}}. \quad (6)$$

In this work, the optimal RIS placement is analyzed in the absence of misalignment and, therefore, (6) will be used in the power calculations. To account for misalignment, one can use (2) instead.

III. Static UE

The optimal placement for the RIS is the one that, among all available choices, ensures the maximum possible power at the position of the UE. In the case of a static UE, this can be simply determined by finding the position of the RIS that maximizes (1), using the power density given by (6). As an example, in Fig. 2(a), a 4 × 5 m room is shown in which there are four possible positions for the RIS, a static UE, and one AP, whose link with the UE is blocked, all on the same

plane. The black dashed-dotted line denotes the blocked LoS of the AP to the UE, the vertical dashed lines mark the normal from the RIS surface, to denote its orientation, and the rest of the colored lines denote the four possible ways that the LoS path can be restored via the RIS. The operating frequency is 150 GHz, the transmitted power of the AP is 30 dBm, the gain of the UE is 20 dB, and the RIS is large enough to capture the entire footprint of the AP beam. In Fig. 2(b), the received power for each RIS-UE link is calculated as a function of G_t using (1), (5), and (6). With regard to how the AP antenna gain affects the optimal RIS placement, two regimes of interest can be observed, characterized by low antenna gain and high antenna gain. In the low antenna gain regime ($G_t \rightarrow 30$ dB), the optimal RIS placement is closest to the AP, in this case RIS 1 (red color-coded lines), while in the high AP antenna gain regime ($G_t \rightarrow 60$ dB), the optimal placement is close to the UE, in this case RIS 3 (purple color-coded lines). The overall maximum received power is achieved with RIS 3, and it is also the optimal placement of the RIS for an antenna of tunable gain. These observations are in agreement with analytical derivations for the optimal RIS placement using the simple model provided by (6) (see the Appendix for details).

Already with the example of Fig. 2, it becomes evident that the antenna gain of the AP, G_t, is a parameter that greatly affects the received power at the UE. In Fig. 3, the optimal RIS placement on the top wall of the configuration shown in Fig. 2(a) is further studied under tunable AP antenna gain. The AP is placed at $(x_{AP}, y_{AP}, z_{AP}) = (0, 0, 0)$, the UE at $(x_{UE}, y_{UE}, z_{UE}) = (3, 0, 2)$ and the RIS position $(x_{RIS}, y_{RIS}, z_{RIS})$ moves horizontally from (0, 0, 4) to (5, 0, 4). The AP is equipped with a tunable antenna capable of generating highly directional beams with gain ranging from 30 to 60 dB. In Fig. 3(a), the horizontal position x_{RIS} that maximizes the received power is presented as a function of G_t. For low gain, $x_{RIS} = x_{AP}$, i.e., the received power is maximized if the RIS is placed closer to the AP. As G_t increases, the optimal x_{RIS} moves closer to x_{UE}, which is the horizontal position of the UE. When the AP antenna gain reaches 52 dB, the optimal $x_{RIS} = x_{UE}$. Higher gains move the optimal x_{RIS} up to $x_{RIS} = 3.2$ m. The color-coded markers correspond to the four selected examples presented explicitly in Fig. 3(b), where the received power is calculated as a function of x_{RIS}. As the RIS moves from one side of the room to the opposite, the power received by the UE increases until the RIS reaches the optimal x_{RIS} and then decreases. The optimal x_{RIS} is different for each G_t as previously shown. For example, with $G_t = 35$ dB, which is a relatively low antenna gain, the received power reaches the maximum value, -3 dBm, when the RIS is close to the AP ($x_{RIS} = 0.2$ m and $x_{AP} = 0$ m), and decreases when the RIS moves further. By increasing the antenna gain to higher values, the maximum received power is reached when the RIS is closer to the UE ($x_{UE} = 3$ m). With $G_t = 45$ dB, the maximum $P_r = 5.6$ dBm is reached when the RIS is at $x_{RIS} = 1.7$ m; with $G_t = 52$, the maximum $P_r = 9$ dBm is reached at $x_{RIS} = 3$ m; and with $G_t = 55$ dB, the maximum value, 8 dBm, is reached at $x_{RIS} = 3.2$ m. With $G_t = 52$ dB, the overall maximum received power is achieved, and the optimal placement of the RIS is at $x_{RIS} = x_{UE}$.

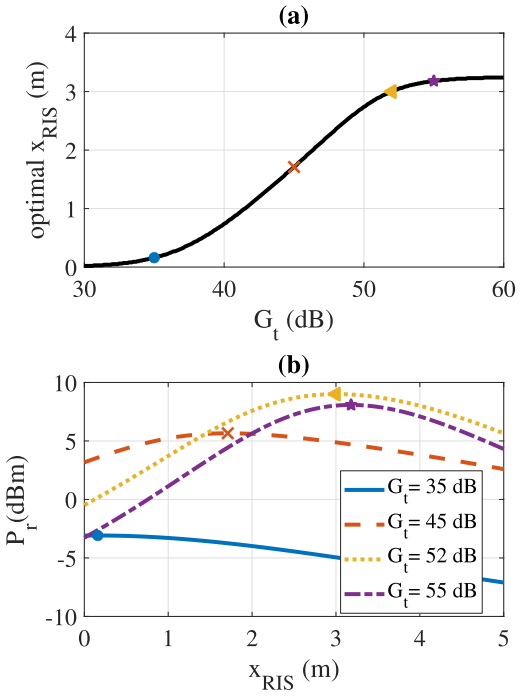

Fig. 3. Optimal RIS placement under tunable AP antenna gain. (a) Position of RIS (x_{RIS}) on the top wall of the configuration shown in Fig. 2(a), at which the received power is maximized, as a function of the AP antenna gain. (b) Received power at the UE as a function of x_{RIS}, for the four cases marked in (a). The UE is placed at (3, 0, 2), the AP is placed at (0, 0, 0), and the RIS moves from (0, 0, 4) to (5, 0, 4).

IV. Mobile UE Environment

The mobility of the UE is one of the main parameters that greatly affects the optimal placement of the RIS, while for a static UE, the optimal RIS placement can be determined uniquely, when the UE moves the RIS position that maximizes the received power depends on the UE position and, hence, the optimal RIS placement involves a multitude of solutions. A straightforward way to find the optimal placement is by imposing a threshold on the minimum desired power received by the UE, for all possible positions of the UE within the expected region of mobility. The outcome of this parametric scan yields ranges for the RIS position that, for increasing threshold, collapse to isolated points, guaranteeing that the calculated RIS placement satisfies the imposed minimum received power threshold for all potential positions of the UE.

A. RIS Placement in Mobile UE Environment

In Fig. 4, three scenarios for the position of the AP in a 4×5 m room are presented for three selected AP antenna gains, namely, 30 dB (left column panels), 40 dB (middle column panels), and 50 dB (right column panels). The position of the AP is marked with a blue cross and affects the available positions for the RIS. For example, if the AP is placed on one of the four walls, to ensure that the RIS captures the AP

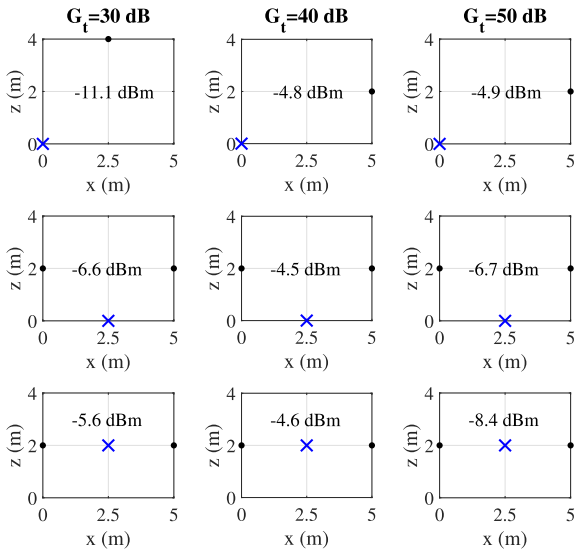

Fig. 4. Optimal RIS placement for different scenarios and AP antenna gains.

beam, the RIS placement is meaningful only on the remaining three walls; similarly, if the AP is placed in a corner, the RIS placement is meaningful only at the opposite two walls. Furthermore, if the RIS is placed at the center of the room, all walls are available for the RIS to be placed at the center of the room. In the calculations, the RIS position is scanned at 10 cm increments while keeping its surface parallel to the wall that it is placed, i.e., the RIS normal always points to the opposite wall. The positions that ensure the maximum received power threshold in each scenario are marked with the black dots and the minimum received power in the entirety of the room that is achieved with the RIS at the marked position is also shown explicitly in each panel. The optimal RIS placement is the same for all scenarios with the exception of the top panel with $G_t = 30$ dB. The optimal RIS placement in this scenario is closer to the AP than with higher values of G_t. By increasing G_t from 30 to 40 dB, the threshold increases, but increasing it from 40 to 50 dB, the threshold decreases. The optimal value of G_t is found to be between 40 and 50 dB.

To gain some insight into the choices dictated by the preceding analysis, it is important to note that, because the RIS is considered to be lossless, the total power reflected by the RIS is the same for all possible UE positions. However, the RIS redistributes the incident power in space and, hence, the optimal RIS placement is determined by the local power density of the reflected beam. This is shown in Fig. 5(a) for all possible UE positions within the illustrated area. The solid lines represent three chosen steering angles, namely, $\theta_{UE} = 0°$ (blue), $\theta_{UE} = 20°$ (red), and $\theta_{UE} = 40°$ (yellow), and the dashed line marks their values at distance $z = 3$ m; the contour lines represent the locus of UE positions, where the same received power can be achieved for each individual case. The spatial distribution of the received power for the chosen angles along the dashed line is shown in Fig. 5(b). What is actually observed is that, with increasing θ_{UE}, the beam undergoes stronger spreading, thus resulting in reduction in its peak power and, consequently, in the received power (in

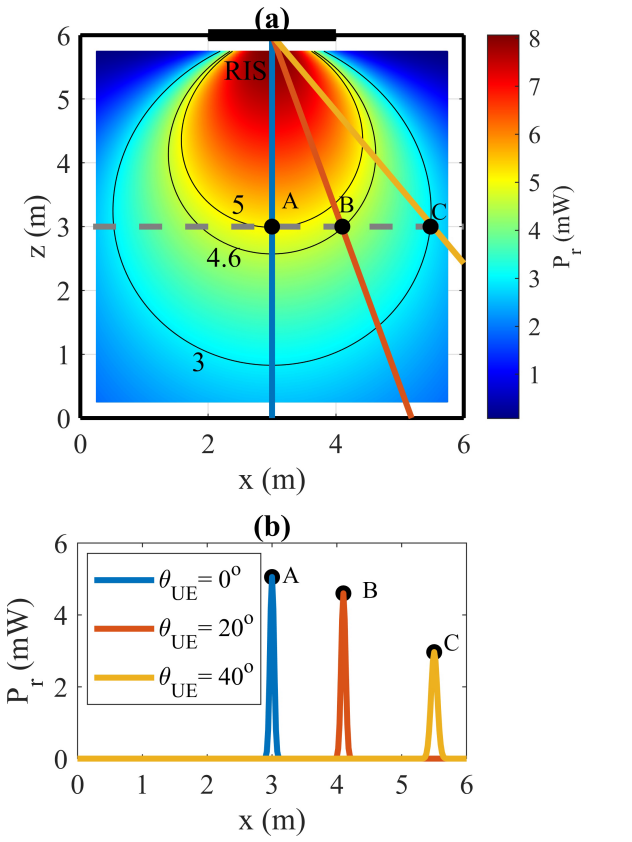

Fig. 5. Spatial distribution of received power. (a) Received power as a function of the UE position in the absence of misalignment and (b) cross section at $z = 3$ m for the cases marked at (a) with steering angle $\theta_{UE} = 0°$, 20°, and 40°; points A, B, and C mark the peak power for each case. The contour lines represent the locus of UE positions, where the same received power can be achieved for each individual case. The radius of the footprint of the AP beam on the RIS w_{RIS} is 5 cm.

the absence of misalignment, the UE is located at the peak of each distribution).

The spatial power distribution shown in Fig. 5 provides a simple and intuitive explanation with respect to the choice for the optimal RIS placement: each contour line marks a certain power threshold, P_{th}, and the area enclosed by the contour line guarantees a minimum received power of P_{th}. Therefore, the determination of the RIS position that satisfies a certain power threshold can be solved geometrically, i.e., by searching for the distance, within which the UE must be located so that $P_r \geq P_{th}$. This threshold distance, d_{UE}^{th}, can be expressed analytically by using (6) to solve (1) in terms of $d_{UE} \equiv d_{UE}^{th}$

$$d_{UE}^{th}(P_{th}) = z_R \sqrt{a(P_{th}) - \frac{1 + \cos^4 \theta_{UE}}{2}} \tag{7}$$

where

$$a(P_{th}) = \sqrt{\left(\frac{P_t}{P_{th}} \frac{2A_r |R|^2}{\lambda z_R} \cos^2 \theta_{UE}\right)^2 + \left(\frac{1 - \cos^4 \theta_{UE}}{2}\right)^2}. \tag{8}$$

Note that the result of (7) reproduces analytically the contour lines shown in Fig. 5(a) using $P_{th} = 3, 4.6$, and 5 mW. The geometric perspective provided by the above analysis is

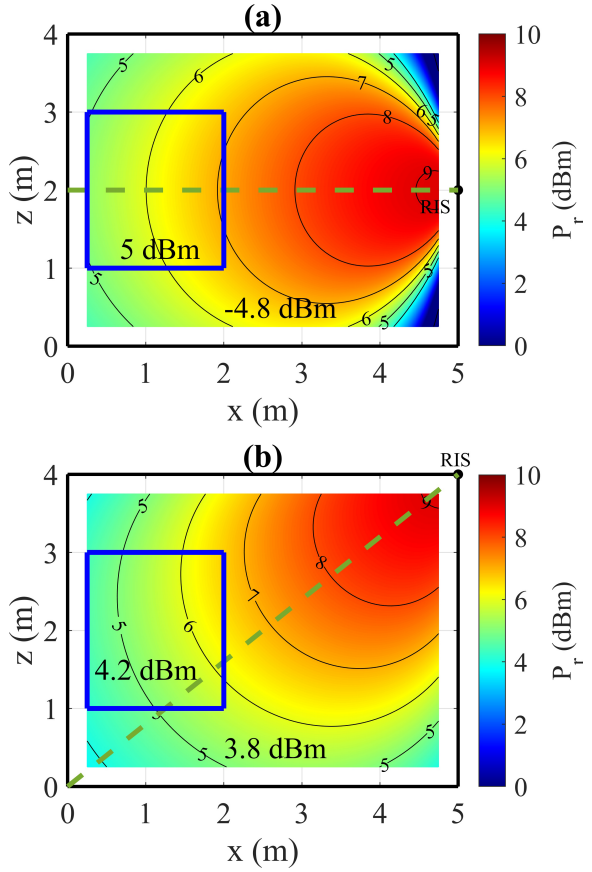

Fig. 6. Received power in a 4 × 5 room with different RIS placements and orientations that are depicted with the green dashed lines. The radius of the AP footprint on the RIS is $w_{RIS} = 5$ cm, and the minimum received power within each area of interest (entire room or rectangular area marked with the blue box) is also shown.

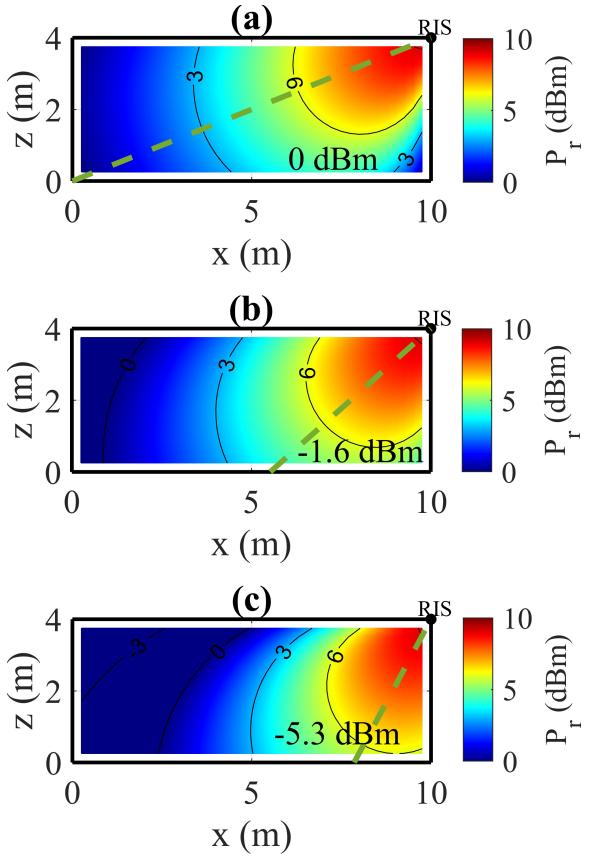

Fig. 7. Received power in a 4 × 10 m room with different RIS orientations that are depicted with the green dashed lines and $w_{RIS} = 5$ cm. (a) RIS normal is oriented toward the opposite corner of the room. (b) RIS is rotated counterclockwise by 20°. (c) RIS is rotated another 20°. The received power threshold in the room is shown at the bottom of each panel.

particularly useful for gaining insight into the implications of the RIS orientation on the received power, as will be shown next.

B. Impact of RIS Orientation

The impact of the RIS orientation on the received power can be studied by means of the location of the contour lines provided by (7). As an example, in Fig. 6, the received power is shown in a 4 × 5 m room, for two different placements of the RIS, each with a different orientation. The green dashed lines depict the orientations of the RISs and the blue lines outline a small area of interest in the room. In Fig. 6(a), the RIS is placed at (5, 0, 2), which is the center of the right wall and is oriented toward the center of the left wall, and in Fig. 6(b), it is placed at (5, 0, 4), which is the top-right corner of the room and is oriented toward the opposite corner. The transmitted power is 30 dBm, the antenna gain of the UE is 20 dB, and the radius w_{RIS} of the AP beam footprint on the RIS is 5 cm. As shown in (6), the received power at the UE is affected by both d_{UE} and θ_{UE}, and it decreases with their increase. Therefore, the optimal RIS placement and orientation must jointly minimize both the maximum d_{UE} and the maximum θ_{UE}. In Fig. 6(a), the minimum received power in the entire room is −4.8 dBm and is practically determined by the region close to the RIS, where $\theta_{UE} \approx 90°$. On the other hand, in Fig. 6(b), the RIS orientation relative to the room eliminates this region, therefore providing a higher minimum received power, which reaches 3.8 dBm. In the small areas of interest, marked with blue rectangles, the situation is reversed. In Fig. 6(a), the minimum received power is 5 dBm and the maximum 7 dBm, while in Fig. 6(b), the minimum received power is 4.2 dBm and the maximum 6.8 dBm. The reason is that the RIS in Fig. 6(a) is closer to the area of interest (d_{UE} is relatively short), while the orientation of the RIS provides low θ_{UE} for all the positions inside the area of interest in relation to the RIS in Fig. 6(b). On that account, the optimal position and orientation of the RIS depend on the area of interest that needs to be illuminated by the RIS.

In Fig. 7, the received power levels for all possible positions of the UE are shown for three different orientations of the RIS. In order to emphasize the impact of the orientation, the room in the simulations is long and narrow with dimensions 4 × 10 m. The RIS is placed in the top-right corner of the room and the radius of the footprint of the AP beam on the RIS is $w_{RIS} = 5$ cm. The orientation of the RIS normal is depicted by the green dashed line and the minimum received power is shown at the bottom of each panel. In Fig. 7(a), the RIS normal is oriented toward the opposite corner of

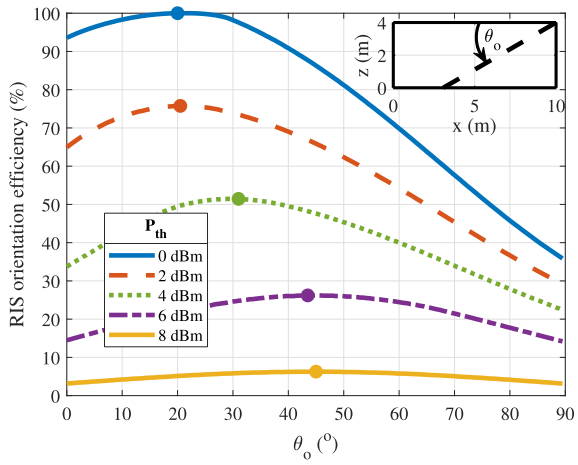

Fig. 8. Room coverage versus orientation angle θ_o for the power thresholds shown in the legend. The room size is 4 × 10 m and the footprint radius of the AP beam on the RIS, w_{RIS}, is 5 cm.

the room; in Fig. 7(b), the RIS is rotated counterclockwise by 20°; and in Fig. 7(c), the RIS is rotated another 20°. By changing the RIS orientation, the power contour levels "move" toward the new direction, but the farther the green dashed line moves from the bottom-left corner, the more areas with large θ_{UE} come into play and the more the threshold of the whole room decreases. For example, the threshold is 0 dBm in Fig. 7(a), −1.6 dBm in Fig. 7(b), and −5.3 dBm in Fig. 7(c). Apparently, the optimal RIS orientation is the one where the RIS points toward the opposite corner, i.e., it is the one that eliminates the combination of large angles θ_{UE} with large distances d_{UE}. Therefore, in rectangular rooms as the one examined here, it is preferable to place the RIS in corners. In general, the shape of the room also plays a significant role, as the walls restrict the user's motion. In a square room, by placing the RIS in a corner and it being oriented toward the opposite corner, the maximum possible θ_{UE} is limited to 45°. However, in a rectangular room, with the same RIS placement and orientation, the maximum θ_{UE} increases the more disproportionate the lengths of the walls are. Overall, our study reveals that the optimal orientation of the RIS is toward the opposite corner of the room, where the RIS-UE distance is maximized.

The spatial distribution of the received power shown in Fig. 7 provides some intuitive guidelines with respect to the optimal RIS orientation. For example, with simple inspection, it can be deduced that the RIS orientation with the RIS normal pointing at the opposite corner maximizes the minimum received power within the room. The optimal RIS orientation can also be quantified in terms of room coverage, i.e., the percentage of the room area that lies within the power contour outlined by $d_{UE}^{th}(P_{th})$. Fig. 8 shows the RIS orientation efficiency, expressing the room coverage, versus the orientation angle θ_o for the power thresholds shown in the legend. The angle θ_o is the orientation angle of the RIS normal with respect to the top wall as shown in the inset, and the colored dots mark the maximum efficiency for each threshold. The room is of size 4 × 10 m and the RIS is placed at the top-right corner of the room. For thresholds below 0 dBm, the RIS orientation is irrelevant, and however, with increasing threshold, a unique maximum appears as θ_o is scanned from 0° to 90°. For 0 dBm, the optimal RIS orientation is at 20°, i.e., with the RIS normal pointing toward the opposite corner, as already discussed. Interestingly, for higher thresholds where less than 100% room coverage is achievable, the maximum moves to larger angles, reaching up to 45°. The reason is that, as shown in Fig. 7, high thresholds can only be achieved closer to the RIS, and the power contour lines that mark them fit inside the rectangular shape of the room efficiently at different RIS orientations.

V. Discussion

In real implementations, the RIS elements may be lossy, and they can have nonuniform response with respect to the angle of incidence and can be anisotropic, possibly leading to coupling between the x- and y-polarizations. In this work, in order to provide some insight into the underlying mechanisms that determine the path loss in RIS-assisted links, the complexity of the analytical model was kept minimal by considering ideal RIS operation; the RIS was assumed to be lossless, polarization preserving and with a uniform response with respect to the angle of incidence, essentially accounting for either isotropic RIS elements or linearly birefringent RIS elements with their fast/slow axis oriented along the x-/y-directions, excited by x- or y-polarized beams (in which case polarization mixing does not take place). Even under such ideal RIS operation, a rich performance was demonstrated. To account for effects of nonideal RIS, the power density at the receiver can be directly written as a weighted superposition of the incident power among the two polarizations as

$$\begin{pmatrix} S_x \\ S_y \end{pmatrix} = \begin{pmatrix} a_{xx}(\theta_{AP}) & a_{xy}(\theta_{AP}) \\ a_{yx}(\theta_{AP}) & a_{yy}(\theta_{AP}) \end{pmatrix} \begin{pmatrix} P_{tx} \\ P_{ty} \end{pmatrix} \tag{9}$$

where P_{ti} and S_i are the power of the incident beam and the power density at the receiver, respectively, along the $i = \{x, y\}$ polarization, and the matrix elements a_{ij} are in general different, accounting for effects of linear birefringence (diagonal terms) and circular birefringence (off-diagonal terms). The functional form of a_{ij} is determined by the particular RIS element design. For example, for ideal RIS operation, as considered in the examples of this work, $a_{xy} = a_{yx} = 0$, $a_{xx} = a_{yy} \equiv S_r/P_t$, where S_r is given by (2). A possible dependence on θ_{AP} for a particular RIS design will lead to a global angle-dependent RIS response and can be, therefore, directly introduced as a prefactor in the analytical form of S_r.

The results presented in this work have also been validated using the discrete approach adopted in other works [17], [18], by considering an RIS of 1200 × 1200 elements of size $\lambda/5$ that is large enough to capture the entire incident beam of radius $w_{RIS} = 5$ cm. While both the discrete approach and the analytical model presented here lead to the same results, the fully discrete model requires significantly longer calculation times because the E-field must be calculated at the UE as a sum over all RIS elements, and this calculation must be repeated for every UE and RIS position. More importantly, the calculation complexity increases severely for a tunable AP antenna, if the problem must be solved repeatedly as a function

of the AP gain. However, with the analytical model presented in this work, the calculation complexity is limited to only the extent of the spatial discretization for the possible RIS and UE positions.

Another important benefit of using the analytical approach presented in this work is that, via the power threshold condition, the problem of optimal RIS placement is transformed into a level set problem: if S_{UE} is the set containing all UE positions within the UE mobility area and S_{RIS} is the set containing all UE positions within the contour defined by $d_{UE}^{th}(P_{th})$, then the optimal RIS placement is simply the one that maximizes $S_{UE} \cap S_{RIS}$.

The form of the power contour lines expresses the fact that the received power is stronger at distances close to the RIS and at angles close to the RIS normal. This is a direct consequence of the spreading that the reflected beam undergoes, which depends on the size of the AP footprint; for example, with decreasing w_{RIS}, the beam spreading becomes stronger and the slope of the received power increases at the vicinity of the RIS, while in the opposite case, with increasing w_{RIS}, the slope decreases. Therefore, for smaller w_{RIS}, the received power drops more rapidly as the UE departs from the RIS. Although the analysis was focused on pencil beams with footprint smaller than the RIS area, the conclusions can be extended to wide beams illuminating the entire RIS surface. In this case, because full RIS illumination leads to the generation of sidelobes, the parameter w_{RIS} models the radius of the main lobe reflected from the RIS, which is of relevance when considering the power received by the UE.

It is also important to note that the analysis presented here aims to provide a general framework for assessing the optimal RIS placement and, therefore, the RIS was considered to be lossless ($R = 1$). Real RIS implementations are expected to impose loss due to undesired scattering and absoprtion, which can possibly depend on the steering angle θ_{UE}. Any such loss can be directly incorporated in the analytical expressions via the parameter R.

In this work, a general methodology for assessing the optimal RIS placement is presented that goes beyond the particular details of the topology, and therefore, a criterion based on the minimum received power of the deterministic channel was used. Any stochastic aspects will be associated with the particular topology. By dressing the deterministic (2) with the appropriate PDF, the system model can be extended in a straightforward manner to a system model suitable for stochastic analysis.

VI. Conclusion

In this work, the placement of the RIS in RIS-aided links was studied with respect to both optimal position and orientation. The analysis was based on an analytical model that treats the RIS as a continuous surface of finite size, rather than a planar distribution of discrete scatterers. Using this approach, simple analytical expressions were derived, which explain how the AP gain affects the optimal RIS placement for a static user and provide insight into how a minimum received power is ensured for a user that is free to move within a certain area. The findings were demonstrated with D-band indoor examples and can be extended to outdoor scenarios of any targeted frequency. The approach adopted in this work provides direct visualization of how the incident power is redistributed in the available space, thus facilitating the understanding of how the choices for optimal RIS placement have to be made.

Appendix

A. Analytical Derivation of Optimal RIS Placement

1) Low Gain Limit: In the limit of low gain, $d_{UE}/z_R \ll 1$, and the received power acquires the simple form

$$P_r = A_r \frac{2P_t}{\lambda z_R} |R|^2 \tag{10}$$

where z_R is given by (5), i.e., $z_R = 4kd_{AP}^2/G_t$, repeated here for convenience. The distance d_{AP} is

$$d_{AP}^2 = (x_{AP} - x_{RIS})^2 + (z_{AP} - z_{RIS})^2 \tag{11}$$

where $(x_{AP}, 0, z_{AP})$ and $(x_{RIS}, 0, z_{RIS})$ are the coordinates of the AP and RIS positions, respectively, in the configuration of Fig. 2(a). Replacing (11) into (10) and differentiating with respect to x_{RIS}, the maximum power is found for $x_{RIS} = x_{AP}$. Hence, for low gain, the optimal RIS placement is close to the AP, as shown in the example of Fig. 3.

2) High Gain Limit: In the limit of high gain, $d_{UE}/z_R \gg 1$, and the received power acquires the simple form

$$P_r = A_r \frac{2P_t}{\lambda} |R|^2 \frac{\cos^2\theta_{UE}}{d_{UE}^2} z_R. \tag{12}$$

The distance d_{UE} is

$$d_{UE}^2 = (x_{UE} - x_{RIS})^2 + (z_{UE} - z_{RIS})^2 \tag{13}$$

where $(x_{UE}, 0, z_{UE})$ are the coordinates of the UE in the configuration of Fig. 2(a). Also,

$$\cos^2\theta_{UE} = \frac{(z_{UE} - z_{RIS})^2}{(x_{UE} - x_{RIS})^2 + (z_{UE} - z_{RIS})^2}. \tag{14}$$

Substituting (13) and (14) into (12) and differentiating with respect to x_{RIS}, the maximum power is found for $x_{RIS} = x_{UE} + \delta x$, with $\delta x < x_{UE}$. Hence, for high gain, the optimal RIS placement is close to the UE, as shown in the example of Fig. 3.

3) Optimal Gain: Between the two limit cases, there is an optimal gain for which the received power is maximized, as shown in Fig. 2(b). The received power at the optimal gain is expressed as [16]

$$P_r = A_r \frac{2P_t}{\lambda d_{UE}} |R|^2 \frac{\cos^2\theta_{UE}}{1 + \cos^2\theta_{UE}}. \tag{15}$$

Substituting (13) and (14) into (15) and differentiating with respect to x_{RIS}, the maximum power is found for $x_{RIS} = x_{UE}$.

References

[1] J. Kokkoniemi, J. Lehtomäki, and M. Juntti, "A line-of-sight channel model for the 100–450 gigahertz frequency band," *EURASIP J. Wireless Commun. Netw.*, vol. 2021, no. 1, pp. 1–15, Apr. 2021.

[2] G. Stratidakis, E. N. Papasotiriou, H. Konstantinis, A.-A.-A. Boulogeorgos, and A. Alexiou, "Relay-based blockage and antenna misalignment mitigation in THz wireless communications," in *Proc. 2nd 6G Wireless Summit (6G SUMMIT)*, Mar. 2020, pp. 1–4.

[3] M. Jacob, S. Priebe, R. Dickhoff, T. Kleine-Ostmann, T. Schrader, and T. Kurner, "Diffraction in mm and sub-mm wave indoor propagation channels," *IEEE Trans. Microw. Theory Techn.*, vol. 60, no. 3, pp. 833–844, Mar. 2012.
[4] G. R. MacCartney, S. Deng, S. Sun, and T. S. Rappaport, "Millimeter-wave human blockage at 73 GHz with a simple double knife-edge diffraction model and extension for directional antennas," in *Proc. IEEE 84th Veh. Technol. Conf. (VTC-Fall)*, Sep. 2016, pp. 1–6.
[5] K. Ntontin, M. Di Renzo, and F. Lazarakis, "On the rate and energy efficiency comparison of reconfigurable intelligent surfaces with relays," in *Proc. IEEE 21st Int. Workshop Signal Process. Adv. Wireless Commun. (SPAWC)*, May 2020, pp. 1–5.
[6] A.-A. A. Boulogeorgos and A. Alexiou, "Performance analysis of reconfigurable intelligent surface-assisted wireless systems and comparison with relaying," *IEEE Access*, vol. 8, pp. 94463–94483, 2020.
[7] K. Ntontin, A.-A.-A. Boulogeorgos, D. G. Selimis, F. I. Lazarakis, A. Alexiou, and S. Chatzinotas, "Reconfigurable intelligent surface optimal placement in millimeter-wave networks," *IEEE Open J. Commun. Soc.*, vol. 2, pp. 704–718, 2021.
[8] E. Ibrahim, R. Nilsson, and J. van de Beek, "On the position of intelligent reflecting surfaces," in *Proc. Joint Eur. Conf. Netw. Commun. 6G Summit (EuCNC/6G Summit)*, Jun. 2021, pp. 66–71.
[9] H. Lu, Y. Zeng, S. Jin, and R. Zhang, "Enabling panoramic full-angle reflection via aerial intelligent reflecting surface," in *Proc. IEEE Int. Conf. Commun. Workshops (ICC Workshops)*, Jun. 2020, pp. 1–6.
[10] G. Ghatak, "On the placement of intelligent surfaces for RSSI-based ranging in mm-wave networks," *IEEE Commun. Lett.*, vol. 25, no. 6, pp. 2043–2047, Jun. 2021.
[11] H. Hashida, Y. Kawamoto, and N. Kato, "Intelligent reflecting surface placement optimization in air-ground communication networks toward 6G," *IEEE Wireless Commun.*, vol. 27, no. 6, pp. 146–151, Dec. 2020.
[12] S. Zhang and R. Zhang, "Intelligent reflecting surface aided multi-user communication: Capacity region and deployment strategy," *IEEE Trans. Commun.*, vol. 69, no. 9, pp. 5790–5806, Sep. 2021.
[13] Z. Cui, K. Guan, J. Zhang, and Z. Zhong, "SNR coverage probability analysis of RIS-aided communication systems," *IEEE Trans. Veh. Technol.*, vol. 70, no. 4, pp. 3914–3919, Apr. 2021.
[14] S. Zeng, H. Zhang, B. Di, Z. Han, and L. Song, "Reconfigurable intelligent surface (RIS) assisted wireless coverage extension: RIS orientation and location optimization," *IEEE Commun. Lett.*, vol. 25, no. 1, pp. 269–273, Jan. 2021.
[15] G. Stratidakis, S. Droulias, and A. Alexiou, "An analytical framework for reconfigurable intelligent surfaces placement in a mobile user environment," in *Proc. 19th ACM Conf. Embedded Netw. Sensor Syst.*, New York, NY, USA, Nov. 2021, pp. 623–627, doi: 10.1145/3485730.3494038.
[16] G. Stratidakis, S. Droulias, and A. Alexiou, "Analytical performance assessment of beamforming efficiency in reconfigurable intelligent surface-aided links," *IEEE Access*, vol. 9, pp. 115922–115931, 2021.
[17] A.-A.-A. Boulogeorgos and A. Alexiou, "Coverage analysis of reconfigurable intelligent surface assisted THz wireless systems," *IEEE Open J. Veh. Technol.*, vol. 2, pp. 94–110, 2021.
[18] W. Tang *et al.*, "Wireless communications with reconfigurable intelligent surface: Path loss modeling and experimental measurement," *IEEE Trans. Wireless Commun.*, vol. 20, no. 1, pp. 421–439, Jan. 2021.
[19] K. Achouri, M. A. Salem, and C. Caloz, "General metasurface synthesis based on susceptibility tensors," *IEEE Trans. Antennas Propag.*, vol. 63, no. 7, pp. 2977–2991, Jul. 2015.
[20] A. Pitilakis *et al.*, "A multi-functional reconfigurable metasurface: Electromagnetic design accounting for fabrication aspects," *IEEE Trans. Antennas Propag.*, vol. 69, no. 3, pp. 1440–1454, Mar. 2021.
[21] G. Oliveri, P. Rocca, M. Salucci, and A. Massa, "Holographic smart EM skins for advanced beam power shaping in next generation wireless environments," *IEEE J. Multiscale Multiphys. Comput. Techn.*, vol. 6, pp. 171–182, 2021.
[22] G. Oliveri, F. Zardi, P. Rocca, M. Salucci, and A. Massa, "Building a smart EM environment -AI-enhanced aperiodic micro-scale design of passive EM skins," *IEEE Trans. Antennas Propag.*, p. 1, 2022.
[23] Y. Hadad and T. Melamed, "Non-orthogonal domain parabolic equation and its tilted Gaussian beam solutions," *IEEE Trans. Antennas Propag.*, vol. 58, no. 4, pp. 1164–1172, Apr. 2010.

Giorgos Stratidakis (Member, IEEE) was born in Athens, Greece, in 1990. He received the bachelor's degree in telecommunications engineering from the Department of Telecommunications Science and Technology, University of Peloponnese, Tripoli, Greece, in 2016, and the master's degree in digital communications and networks from the Department of Digital Systems, University of Piraeus, Piraeus, Greece, in 2018, where he is currently pursuing the Ph.D. degree in wireless communications.

In 2017, he joined the Department of Digital Systems, University of Piraeus, where he conducts research in the area of wireless communications.

Sotiris Droulias received the Diploma degree in electrical and computer engineering and the Ph.D. degree in nonlinear photonics from the National Technical University of Athens, Athens, Greece, in 2001 and 2007, respectively.

He is currently a Research Associate at the Department of Digital Systems, ICT School, University of Piraeus, Piraeus, Greece. From 2012 to 2020, he was a member of the Photonic- Phononic- and Meta-Materials Group, FORTH-IESL, Crete, Greece. From 2009 to 2012, he worked as an Adjunct Lecturer at the University of Patras, Patras, Greece. He has worked on several EC-funded projects. His research interests include metamaterials, photonic crystals, metasurfaces, nanolasers, plasmonics, and active media. He is an author of more than 30 articles and two book chapters.

Dr. Droulias has received more than 15 talk invitations in prestigious conferences. He serves as a reviewer in several scientific journals. In 2019, he received the Best Poster Award for his work on metasurface lasers in META 2019, Lisbon, Portugal. In 2020, he was recognized as an Outstanding Reviewer by the Institute of Physics (IOP).

Angeliki Alexiou (Member, IEEE) received the Diploma degree in electrical and computer engineering from the National Technical University of Athens, Athens, Greece, in 1994, and the Ph.D. degree in electrical engineering from the Imperial College of Science, Technology and Medicine, University of London, London, U.K., in 2000.

Since May 2009, she has been a Faculty Member with the Department of Digital Systems, where she conducts research and teaches undergraduate and postgraduate courses in broadband communications and advanced wireless technologies. She is currently a Professor with the Department of Digital Systems, ICT School, University of Piraeus, Piraeus, Greece. Prior to this appointment, she was with Bell Laboratories, Wireless Research, Lucent Technologies (later Alcatel-Lucent, now NOKIA), Swindon, U.K., first as a member of Technical Staff from January 1999 to February 2006 and later as a Technical Manager from March 2006 to April 2009. She is the Project Coordinator of the H2020 RRANOVA project (ict-terranova.eu) and the Technical Manager of H2020 ARIADNE project (ict-ariadne.eu). Her current research interests include radio interface for systems beyond 5G, multiple-input–multiple-output (MIMO), terahertz (THz) wireless technologies and reconfigurable intelligent surfaces, efficient resource management for ultradense wireless networks, machine-to-machine communications, and artificial intelligence and machine learning for future wireless systems.

Dr. Alexiou is a member of the Technical Chamber of Greece. She was a co-recipient of the Bell Labs President's Gold Award in 2002 for contributions to the Bell Labs Layered Space-Time (BLAST) Project and the Central Bell Labs Teamwork Award in 2004 for role model teamwork and technical achievements in the IST FITNESS project. She is the Chair of the Working Group on Radio Communication Technologies and the Working Group on High Frequencies Radio Technologies of the Wireless World Research Forum.